CATALYSIS TODAY 241:(Part B) pp. 264-269. (2015)

Synthesis, structural characterisation, and catalytic activity of Mn(II)–protected amino acid complexes covalently immobilised on chloropropylated silica gel

Z. Csendes[a], G. Varga[a], N.V. Nagy[b], É.G. Bajnóczi[c], M. Sipiczki[c], S. Carlson[d], S.E. Canton[d], A. Metzinger[c], G. Galbács[c], P. Sipos[c], I. Pálinkó[a*]

[a] *Department of Organic Chemistry, University of Szeged, Dóm tér 8, Szeged H-6720, Hungary*

[b] *Institute of Molecular Pharmacology, Research Centre for Natural Sciences, Hungarian Academy of Sciences, Pusztaszeri út 59-67, Budapest H-1025, Hungary*

[c] *Department of Inorganic and Analytical Chemistry, University of Szeged, Dóm tér 7, Szeged H-6720, Hungary*

[d] *Max-Lab, Lund University, SE-223 63 Lund, Sweden*

ABSTRACT

In this work the syntheses, structure, superoxide dismutase (SOD) activity and the catalytic use in the oxidative transformations of cyclohexene of covalently grafted Mn(II)–complexes formed with various C-protected amino acid (L-histidine, L-cysteine and L-cystine) ligands is presented. The structural features of the surface complexes were studied by EPR, X-ray absorption, and mid/far IR spectroscopies. The superoxide dismutase activities of the materials were determined in a biochemical test reaction. The obtained materials were used as catalysts for the oxidation of cyclohexene with peracetic acid in acetone. Covalent grafting and building the complex onto the surface of the chloropropylated silica gel were successful in all cases. It was found that in many instances the structures obtained and the coordinating groups substantially varied upon changing the conditions of the syntheses. All the covalently immobilised Mn(II)–complexes displayed superoxide dismutase activity and could catalyse the oxidation of cyclohexene.

Keywords: biomimetic catalysis, silica immobilised Mn(II)–complexes, EPR, XAS, superoxide dismutase activity, cyclohexene oxidation

[*] Corresponding author. Tel.: +36 62 544 288, Fax: +36 62 544 200.
E-mail address: palinko@chem.u-szeged.hu (I. Pálinkó).

1. Introduction

The most active and selective catalysts in nature are the enzymes. They catalyse a wide-range of organic transformations under relatively mild conditions (at near atmospheric pressure, in physiological aqueous solution – these are advantages), but in limited temperature and pressure ranges (these are disadvantages) with very high selectivities (this is rather a disadvantage, since a more promiscuous behaviour may be required for the synthesis of chemicals used in the laboratories and/or in the chemical industry). The advantages can be retained, while the disadvantages can be eliminated by preparing a structural or a functional model of the active site of enzymes [1], among them metalloenzymes, which form the topic of this article.

Previously, numerous homogeneous and heterogeneous [2–5] bioinspired mimics have been synthetised and applied for the oxidation of organic molecules. In these biomimetic catalysts redox-active transition metal ions may be used as the central ion, while amino acids or other molecules, having groups that are able to coordinate to it, as ligands [6]. Immobilising these substances on various supports facilitates the recovery and reusability of the catalyst. So far, mostly zeolites [7–8], silicates [9–10] and polymers [11] have been used as supports. Cyclohexene is a good model substrate for oxidation reactions since it has C=C and C–H bonds as well. The formation of the allylic oxidation products 2-cyclohexene-1-ol and/or 2-cyclohexene-1-one indicates the favoured attack of the activated C–H bond, while if cyclohexene oxide is the main product epoxidation is the primary reaction occurring at the C=C bond [12]. The selectivity of the reaction depends on the applied catalyst, the oxidant, and the solvent.

In order to obtain highly active and selective biomimetic catalysts (the model was the Mn-S(upper)O(xide)D(ismutase) enzyme) Mn(II)–C-protected amino acid (L-histidine, L-cysteine, and L-cystine) complexes were covalently grafted onto chloropropylated silica gel. The structural features of the surface complexes were determined and they were used as catalysts for the oxidation of cyclohexene. Results of this research are described in the followings.

2. Experimental

2.1. Materials and method of synthesis

For the syntheses, C-protected (in form of methylester) L-histidine, L-cysteine and L-cystine, $MnCl_2 \cdot 5H_2O$ and chloropropylated silica gel (SG − particle size: 230–400 mesh, BET surface area: 500 m^2/g, functionalisation: 8%)] were used. These materials as well as the 2-propanol solvent were the products of Aldrich Chemical Co. All the chemicals were of analytical grade and were used without further purification.

Even though the preparation method of these types of anchored complexes have been described previously [13–14], for the sake of easier tracking the followings, let us briefly repeat the main points, and give the notations.

First, the support was covalently grafted *via* an N-alkylation reaction by the C-protected amino acids. Then, it was treated with Mn^{2+}-containing solution and the solid material was isolated. At his point, a substance was in our hands that only contained surface-anchored ligands. This is called a surface-grafted complex synthesised under ligand-poor conditions, and will be referred as SG−C-protected amino acid−Mn(II). If this material was further treated in a solution containing excess amount of amino acids, then a surface-grafted complex was obtained under ligand-excess conditions, and will be referred as SG−C-protected amino acid−Mn(II)−C-protected amino acid.

2.2. Analytical measurements

The amount of metal ions on the surface modified silica gel was measured by an Agilent 7700x ICP-MS. Before measurements, the anchored complexes were digested by adding cc. H_2SO_4 then they were diluted with distilled water and filtered.

The nitrogen content of the samples was determined by the Kjeldahl method.

2.3. EPR measurements

EPR spectra of powder samples were recorded with a BRUKER EleXsys E500 spectrometer (microwave frequency 9.51 GHz, microwave power 12 mW, modulation amplitude 5 G, modulation frequency 100 kHz) in quartz EPR tubes. All recorded EPR spectra were simulated with a spectrum decomposition method by the EPR [15] computer program. Analysis of the obtained spectra was significantly helped with the information published concerning the EPR spectra of various Mn(II)−amino acid complexes [16].

2.4. X-ray absorption measurements

The measurements were carried out on the K-edge of the manganese at MAX-lab at beamline I811. This is a superconducting multipole wiggler beamline equipped with a water-cooled channel cut Si(111) double crystal monochromator delivering at 10 keV, approximately 2×10^{15} photons/s/0.1% bandwidth with horizontal and vertical FWHM of 7 and 0.3 mrad, respectively [17]. A beamsize of 0.5 mm × 1.0 mm (width × height) was used. The incident beam intensity (I_0) was measured with an ionisation chamber filled with a mixture of He/N_2. Higher order harmonics were reduced by detuning the second monochromator to 70% of the maximum intensity. Data collection was performed in transmission mode. The samples were contained in Teflon spacers with Kapton tape windows according to the manganese concentration. The data were treated by the Demeter program package [18].

2.5. FT-IR spectroscopy

Structural information on each step of the synthesis procedure was obtained by far- and mid-range infrared spectroscopy. Mid-range spectra were recorded with a BIO-RAD Digilab Division FTS-65 A/896 FT-IR spectrophotometer with 4 cm^{-1} resolution, measuring diffuse reflectance. The 3800–600 cm^{-1} wavenumber range was investigated. 256 scans were collected for each spectrum.

Far-range spectra were recorded with a BIO-RAD Digilab Division FTS-40 vacuum FT-IR spectrophotometer with 4 cm^{-1} resolution. 256 scans were collected for each spectrum. The Nujol mull technique was used. The 500–200 cm^{-1} wavenumber range was investigated. Spectra were evaluated by the Win-IR package. They were baseline-corrected, smoothed (if it was necessary) and the spectra of supports were subtracted. Interpretation of the spectra was helped either by published mid IR results [19, 20] and our own freshly published experimental work concerning the far IR spectra of purpose-built manganese complexes having uniform coordinating groups [21].

2.6. Testing the catalytic activity

Superoxide dismutase activity was tested by the Beauchamp-Fridovich reaction [22]. For this biochemical test reaction riboflavin, L-methionine, and nitro blue tetrazolium (NBT) were used as was described previously [13] with the exception that in this case HEPES buffer was used. During their reaction, superoxide radical anions are formed, which gives blue adducts with NBT. When the enzyme mimic is present, it dismutates the superoxide radical anion, the photoreduction of NBT is inhibited (its measure is IC_{50} in mM), *i.e.* the enzyme mimic works the better when the colour change (measured by the absorbance), *i.e.* the value of IC_{50}, is the smaller.

2.7. Catalytic oxidation of cyclohexene

In the reaction a vial capped with septum was loaded with the catalyst (25 mg), acetone (10 cm^3), cyclohexene (5 mmol) and peracetic acid (1 mmol). After 1 h continuous stirring at room temperature (298 K), the mixture was analysed quantitatively by GC using an Agilent HP-1 column. The products were identified by GC–MS.

3. Results and discussion

3.1. Analytical measurements

The results of the Kjeldahl method and the ICP–MS measurements are shown in Table 1.

Table 1

Covalent grafting of the amino acids was successful in all cases. The conversion of the immobilisation is ranged from 57−86 %, since the chloropropylated silica gel contained 0.705 mmol/g active chlorine. The metal ion to amino acid ratio under ligand-poor conditions is 1:1.5 for SG–His-OMe–Mn(II) suggesting that complexes formed on the surface are not uniform, there are complexes having 1:1 as well as 1:2 metal ion to ligand ratios. For SG–Cys-OMe–Mn(II) this ratio is 1:1 and for SG–$(Cys\text{-}OMe)_2$–Mn(II) is 1:1.1, meaning that mainly 1:1 complexes are formed. Under ligand-excess conditions, this ratios are 1:5.4, 1:3.2 and 1:2.5 for SG–His-OMe–Mn(II)–H-His-OMe, SG–Cys-OMe–Mn(II)–H-Cys-OMe and SG–$(Cys\text{-}OMe)_2$–Mn(II)–H-$(Cys\text{-}OMe)_2$, respectively. It seems that in all cases mixture complexes with varying coordination numbers were formed on the surface of the support.

3.2. EPR measurements

All EPR spectra (Fig. 1), recorded for the different amino acid containing samples, could be characterised by the superposition of a very broad singlet signal and a well-resolved signal of six lines. The broad signal (g_{iso} = 2.013 ± 0.003 and linewidth w = 450 ± 130 G) is typical for coupled Mn^{2+} centres for which the significant signal broadening is due to the dipolar interactions and a random orientation of the paramagnetic metal ions. The well-resolved component is probably originated from isolated Mn^{2+} centres. The six hyperfine lines with g_{iso} = 1.9985±0.0001 and A_{iso} = 88.5±0.1 G are due to the interaction of the electron spin with the nuclear spin (^{55}Mn, I = 5/2). The observed g values are very close to the free electron g value, suggestive of the absence of spin orbit coupling in the ground state. These features are characteristic of oxygen coordinated Mn^{2+} ion in disordered systems and the A_{iso} values suggest that the Mn(II) in the immobilised complexes is in an octahedral coordination environment [23, 24].

Figure 1

3.3. X-ray absorption measurements

Mn K-edge XAS spectra were recorded only for the ligand-poor complexes. The XANES spectra of the materials are displayed in Fig. 2.

Figure 2

The pre-edge feature, corresponding to 1s → 3d transitions around 6540 eV is weak, indicating symmetric geometry and high coordination number, since these transitions are Laporte-forbidden in centrosymmetric environments [25]. This result suggests that the immobilised Mn(II) complexes are octahedral. This data is consistent with the EPR observations.

The EXAFS data were k^3-weighted and Fourier transformed in the range of k = 2−11 $Å^{-1}$. The ranges for the backtransform were 1–3 Å for all complexes. The fitted parameters included the amplitude reduction factor (S_0^2), interatomic distances (R), Debye-Waller factors (σ^2) and energy shift (ΔE_0). The coordination numbers (N) were kept constant during each optimisation, but a range of coordination numbers were used to find the best fit. The k^3-weighted EXAFS spectra are shown in Fig. 3, and the results of the fitting are reported in Table 2.

Figure 3

Table 2

The EXAFS measurement revealed that six oxygen/nitrogen atoms (by these measurements the difference between oxygen and nitrogen cannot be estimated clearly, they scatter the photoelectrons nearly the same way, due to their similar atomic masses) form the first coordination sphere of SG–His-OMe–Mn(II), where the Mn(II)–O/N bond distance was fitted to be 2.18 Å. In SG–$(Cys\text{-}OMe)_2$–Mn(II) the first coordination shell contains six oxygen/nitrogen atoms as well with a Mn(II)–O/N bond length of 2.19 Å. For SG–Cys-OMe–Mn(II) two different interatomic distances can be distinguished in the first shell. The first one corresponds to the Mn(II)–O/N distance of 2.21 Å with a coordination number of five, while the second peak is related to a Mn(II)–S distance (R = 2.64 Å), where the coordination number is one. These results are similar to those obtained with Mn(II) ion coordinated with various carboxylates or histidine as ligands [26].

3.4. FT-IR spectroscopy

The coordinating groups were identified through comparing the difference mid IR spectra (the spectrum of the support was subtracted) of the silica gel grafted amino acids and the difference spectra of the immobilised complexes prepared under ligand-poor conditions or the spectra of the pristine amino acids and the difference spectra of the anchored complexes prepared under ligand-excess conditions.

The mid IR difference spectra of the silica gel anchored amino acids (Figs. 4, 6, 8 trace A) show that in all cases carboxylate vibrations appeared. It means that the C-protecting group hydrolysed upon covalent anchoring due to the basic conditions and is present as carboxylate group in the samples.

Figure 4

In the difference spectrum of SG–(His-OMe) the $\nu_{asym(COO-)}$ and $\nu_{sym(COO-)}$ stretching frequencies can be seen at 1582 cm^{-1} and 1412 cm^{-1}, respectively (Fig 4, trace A). To assign the $\nu_{sym(COO-)}$ vibrations, Raman spectra (not shown) were registered as well, since these vibrations are more intense there. The difference Δ [$\Delta = \nu_{asym(COO-)} - \nu_{sym(COO-)}$] is 170 cm^{-1} here, while it is found to be 146 cm^{-1} [Δ = 1588 – 1442 cm^{-1}] for the ligand poor complex (Fig. 4, trace B), suggesting that the carboxylate group appears in the coordination sphere of the metal ion as bidentate ligand [27]. The band at 259 cm^{-1} in the far IR spectrum of the material (Fig. 5, trace A) indicates that the imidazole nitrogen takes part in the complexation,

the vibrations at 350 and 326 cm^{-1} correspond to the Mn–$O_{carboxylate}$ vibrations, while the bands above 400 cm^{-1} can be assigned as the Mn−coordinated water vibrations [28], originated from the crystal water of the Mn salt.

Figure 5

Adding C-protected histidine in excess (Fig. 4, trace C) resulted in the rearrangement of the surface-grafted ligand-poor complex. This spectrum is very similar to that of the pristine C-protected histidine (trace D), the carbonyl band did not move, meaning that the carbonyl oxygen is not coordinated to the centre ion. The Mn(II)–$N_{imidazole}$ vibration is observed at 266 cm^{-1}, the bands above 400 cm^{-1} can be assigned as coordinated water vibrations (Fig. 5, trace B). Kjeldahl measurement showed that the metal:ligand ratio is 1:5.4, now it is clear that maximum three histidine molecules can coordinate, since the surface grafted histidine saturates three positions in the coordination sphere, there is a water molecule in another position, thus two free position remain for the added C-protected histidine molecules. Consequently, there are non-coordinating histidine molecules on the surface of the silica gel.

In the case of SG–Cys-OMe–Mn(II) (Fig 6, trace B), Δ is 1610 – 1409 cm^{-1} = 201 cm^{-1} suggesting the monodentate ligation of the carboxylate group. There is no S−H vibration at around 2500 cm^{-1}; therefore, the thiolate sulphur is coordinated, as it was also learnt from the XAS measurement. In the far IR range (Fig. 7, trace A), the broad band between 360–300 cm^{-1} indicates the coordination of the carboxylate oxygen and the thiolate sulphur. Under ligand-excess conditions (Fig. 6, trace C), the carbonyl oxygen does not take part in the complexation, since the position of the band does not move relative to the pristine amino acid (Fig. 6, trace D). The lack of the S−H vibration proves that the thiolate group is coordinated to the manganese ion. In the far IR range (Fig. 7, trace B) a broad band can be seen between 370 and 300 cm^{-1} corresponding to the Mn(II)–$S_{thiolate}$ and Mn(II)–$O_{carboxylate}$ vibrations. The bands above 400 cm^{-1} can be assigned as the Mn−coordinated water vibrations, originated from the crystal water of the Mn salt.

Figures 6 and 7

As far as SG–$(Cys\text{-}OMe)_2$–Mn(II) is concerned (Fig 8, trace B) the carboxylate groups are coordinated as monodentate ligands, since Δ increased from 185 cm^{-1} (trace A) to 204 cm^{-1}. In the far IR range, the peak at 354 cm^{-1} corresponds to the Mn–$O_{carboxylate}$ vibration. Under ligand-excess conditions (trace C) the carbonyl oxygens are not involved in the coordination, since the stretching vibrations of the carbonyl bands (1746 and 1734 cm^{-1}) did

not shift to lower wavenumbers. This is the reason why the added C-protected cystine molecules were coordinated with their amino nitrogens. It was confirmed by far IR measurement, since a new band appeared at 378 cm^{-1} due to the coordination of amino nitrogen [29].

Figure 8

Putting together all the information, structural proposals for the surface-bound complexes are offered as follows:

SG–His-OMe–Mn(II)

$N_{imidazoleHissurf}O_{carboxylateHissurf}O_{carboxylateHissurf}H_2O,H_2O,H_2O$, SG–His-OMe–Mn(II)–H-His-OMe

$N_{imidazoleHissurf}O_{carboxylateHissurf}O_{carboxylateHissurf}N_{imidazoleHis},N_{imidazoleHis}H_2O$, SG–Cys-OMe–Mn(II)

$S_{thiolateCyssurf}O_{carboxylateCysssurf}H_2O,H_2O,H_2O,H_2O$, SG–Cys-OMe–Mn(II)–H-Cys-OMe

$S_{thiolateCyssurf}O_{carboxylateCysssurf}S_{thiolateCys}S_{thiolateCys}H_2O,H_2O$, SG–$(Cys\text{-}OMe)_2$–Mn(II)

$O_{carboxylate(Cys)2surf}$ $O_{carboxylate(Cys)2surf}$ H_2O,H_2O,H_2O,H_2O SG–$(Cys\text{-}OMe)_2$–Mn(II)–$(H\text{-}Cys\text{-}OMe)_2$

$O_{carboxylate(Cys)2surf}$ $O_{carboxylate(Cys)2surf}$ $N_{amino(Cys)2}N_{amino(Cys)2}H_2O,H_2O$,

where ‘surf’ stands for surface.

3.5. Superoxide dismutase activity

All materials displayed catalytic activity, *i.e.*, could catalyse the dismutation of the superoxide radical anion. Catalytic activities are close to each other (Table 3). It seems that all the immobilised complexes promote this reaction similarly. The superoxide dismutase activities do not depend on the coordinating groups. The most active anchored complex was found to be SG–His-OMe–Mn(II)–H-His-OMe.

Table 3

3.6. Catalytic oxidation of cyclohexene

The conversion and selectivity results of the immobilised catalysts on the oxidation of cyclohexene with peracetic acid in acetone are reported in Table 4.

Table 4

The expected reactions are the epoxidation, the isomerisation, and the oxidative ring opening of the epoxide ring producing diols. Similar reactions were identified with binuclear Mn(II)−amino acid based complexes encapsulated in zeolite Y, when H_2O_2 was the oxidising agent [30]. The manganese complexes are probably active in the decomposition of peroxides, *i.e.* that of the peracetic acid as well. Fortunately, in acetone, the peroxide is protected against decomposition [31]; therefore, acetone was the chosen solvent. This protective property was checked, our immobilised complexes did not promote the decomposition of peracetic acid. Peracetic acid alone (without any catalyst) is a known epoxidation agent. Indeed, epoxidation did occur in our hands as well. The conversion was low, however (Table 4, first entry). In the presence of our immobilised manganese complexes, the transformation of cyclohexene accelerated appreciably, even if conversions over the various immobilised complexes differed significantly. Moreover, the epoxide selectivity also increased considerably relative to the uncatalysed transformation. All the grafted complexes displayed catalytic activity and were selective to cyclohexene oxide formation. The highest activity (50 % conversion) as well as epoxide selectivity (89 %) was reached over SG–His-OMe–Mn(II)–H-His-OMe. The catalysts did not undergo any colour change during the reaction and there was no leaching of the ligands or the complex either.

4. Conclusions

Characterisation by various forms of spectroscopies revealed that the syntheses of the Mn(II)–amino acid complexes were successful in each case. It was found that the imidazole nitrogen, the thiolate sulphur, and the carboxylate oxygen always participated in the complexation, while in one case the amino nitrogen was coordinated to the metal ion as well. The structure of the complexes made under ligand-poor conditions differed from that of complexes made under ligand-excess conditions. All the covalently immobilised complexes were octahedral. Each material displayed SOD activity. The most active complex was the SG–His-OMe–Mn(II)–H-His-OMe. In the oxidation reactions of cyclohexene, using our catalysts the major product was cyclohexene oxide. In many cases, the epoxide selectivity was more than 85 %, while the conversions differed widely. The most active and selective substance was the SG–His-OMe–Mn(II)–H-His-OMe in this reaction as well.

Acknowledgments

This research was financed by the TÁMOP 4.2.2.A-11/1/KONV-2012-0047 grant. Z. Cs gratefully acknowledges the support of TÁMOP 4.2.4.A/2-11-1-2012-0001 ‘National Excellence Program’. The projects are supported by the European Union and the State of Hungary, and co-financed by the European Social Fund.

References

[1] D. J. Xuereb, R. Raja, Catal. Sci. Technol. 1 (2011) 517–534.

[2] L. Que Jr, W. B. Tolman, Nature 455 (2008) 333–339.

[3] Ag. Stamatis, P. Doutsi, Ch. Vartzouma, K.C. Christoforidis, Y. Deligiannakis, M. Louloudi, J. Mol. Catal. A: Chem. 297 (2009) 44–53.

[4] M. C. Esmelindro, E. G. Oestreicher, H. Marquez-Alvarez, C. Dariva, S.M.S. Egues, C. Fernandes, A.J. Bortoluzzi, V. Drago, O.A.C. Antunes, J. Inorg. Biochem. 99 (2005) 2054–2061.

[5] M. Luechinger, A. Kienhöfer, G.D. Pirngruber, Chem. Mater. 18 (2006) 1330–1336.

[6] A.R. Silva, T. Mourão, J. Rocha, Catal. Today 203 (2013) 81–86.

[7] I. Kuzniarska-Biernacka, K. Biernacki, A.L. Magalhães, A.M. Fonseca, I.C. Neves, K. Catal. 278 (2011) 102–110.

[8] B.M. Weckhuysen, A.A. Verberckmoes, L. Fu, R.A. Schoonheydt, J. Phys. Chem. 100 (1996) 9456–9461.

[9] D. Zois, C. Vartzouma, Y. Deligiannakis, N. Hadjiliadis, L. Casella, E. Monzani, M. Louloudi, J. Mol. Catal. A: Chem. 261 (2007) 306–317.

[10] L. Frunz, R. Prins, G.D. Pirngruber, Chem. Mater. 19 (2007) 4357–4366.

[11] S.M. Islam, P. Mondal, S. Mukherjee, A.S. Roy, A. Bhaumik, Polym. Adv. Technol. 22 (2011) 933–941.

[12] M. Salavati Niassary, F. Farzaneh, M. Ghandi, L. Turkian, J. Mol. Catal. A: Chem. 157 (2000) 183–188.

[13] Z. Csendes, V. Bugris, L. Lackó, I. Labádi, J.T. Kiss, I. Pálinkó, Anal. Bioanal. Chem. 397 (2010) 549–555.

[14] Z. Csendes, I. Lajter, V. Bugris, J.T. Kiss, I. Pálinkó, Vibr. Spectrosc. 53 (2010) 132–135.

[15] A. Rockenbauer, L. Korecz, Appl. Magn. Reson. 10 (1996) 29–43.

[16] E. Tiezzi, J. Chem. Soc., Perkin Trans. 2 (1975) 769−773.

[17] S. Carlson, M. Clausen, L. Gridneva, B. Sommarin, C. Svensson, J. Synchrotron Radiat. 13 (2006) 359–364.

[18] B. Ravel, M. Newville, J. Synchrotron Radiat. 12 (2005) 537–541.

[19] A. Arkowska, W. Wojciechowski, Z. Neorg. Khim. 30 (1985) 1438−1442.

[20] I. Grecu, R. Sandulescu, M. Neamtu, Rev. Chim. 37 (1986) 589−595.

[21] G. Varga, Z. Csendes, G. Peintler, O. Berkesi, P. Sipos, I. Pálinkó, Spectrochim. Acta, A http://dx.doi.org/10.1016/j.saa.2013.11.082.
[22] C. Beauchamp, I. Fridovich, Anal. Biochem. 44 (1971) 276–287.
[23] S. K. Misra, Physica B Condens. Matter 203 (1994) 193–200.
[24] P.F. Rapheal, E. Manoj, M.R. Prathapachandra Kurup, Polyhedron 26 (2007) 5088–5094.
[25] Y. Tao, J.E. Shokes, W.C. McGregor, R.A. Scott, R.C. Holz, J. Inorg. Biochem. 111 (2012) 157–163.
[26] D.R. Fernando, T. Mizuno, I. E. Woodrow, A.J.M. Baker, R.N. Collins, New Phytologist 188 (2010) 1014–1027.
[27] G.B. Deacon, R.J. Phillips, Coordin. Chem. Rev. 33 (1980) 227–250.
[28] S.F. Parker, K. Shankland, J.C. Sprunt, U.A. Jayasooriya, Spectrochim. Acta, Part A 53 (1997) 2333–2339.
[29] G.W. Rayner Canham, A.B.P. Lever, Can. J. Chem. 50 (1972) 3866–3871.
[30] M. Ghorbanloo, S. Rahmani, H. Yahiro, Transition Met. Chem. 38 (2013) 725−732.
[31] D.E. De Vos, B.F. Sels, P.A. Jacobs, Cattech 6 (2002) 14–29.

Legends to Figures

Fig. 1 Experimental (black line) and simulated (red line) EPR spectra of A – SG–His-OMe–Mn(II), B – SG–His-OMe–Mn(II)–H-His-OMe, C – SG–Cys-OMe–Mn(II), D – SG–Cys-OMe–Mn(II)–H-Cys-OMe, E – SG–(Cys-OMe)2–Mn(II), F – SG–(Cys-OMe)2–Mn(II)–H-(Cys-OMe)$_2$.

Fig. 2 Mn K-edge XANES spectra of A – SG–His-OMe–Mn(II), B – SG–Cys-OMe–Mn(II), C – SG–(Cys-OMe)$_2$–Mn(II) immobilised complexes.

Fig. 3 k^3-weighted Mn K-edge EXAFS spectra of A – SG–His-OMe–Mn(II), B – SG–(Cys-OMe)$_2$–Mn(II), C – SG–Cys-OMe–Mn(II), red line – fit, black line – experimental.

Fig. 4 IR spectra of A – SG–His-OMe, B – SG–His-OMe–Mn(II), C – SG–His-OMe–Mn(II)–H-His-OMe, D – H-His-OMe. The spectrum of SG is subtracted.

Fig. 5 Far IR spectra of A – SG–His-OMe–Mn(II), B – SG–His-OMe–Mn(II)–H-His-OMe.

Fig. 6 IR spectra of A – SG–Cys-OMe, B – SG–Cys-OMe–Mn(II), C – SG–Cys-OMe–Mn(II)–H-Cys-OMe, D – H-Cys-OMe. The spectrum of SG is subtracted

Fig. 7 Far IR spectra of A – SG–Cys-OMe–Mn(II), B – SG–Cys-OMe–Mn(II)–H-Cys-OMe.

Fig. 8 IR spectra of A – SG–(Cys-OMe)$_2$, B – SG–(Cys-OMe)$_2$–Mn(II), C – SG–(Cys-OMe)$_2$–Mn(II)–H-(Cys-OMe)$_2$, D – H-(Cys-OMe)$_2$. The spectrum of SG is subtracted.

Table 1

Amino acid and Mn^{2+} content of the samples obtained from Kjeldahl type N-determination and ICP-MS measurements.

Sample	Amino acid content (mmol/g)	Mn^{2+} content (mmol/g)
SG–His-OMe–Mn(II)	0.496	0.321
SG–His-OMe–Mn(II)–H-His-OMe	1.726	
SG–Cys-OMe–Mn(II)	0.605	0.607
SG–Cys-OMe–Mn(II)–H-Cys-OMe	1.955	
SG–$(Cys\text{-}OMe)_2$–Mn(II)	0.405	0.363
SG–$(Cys\text{-}OMe)_2$–Mn(II)–H-$(Cys\text{-}OMe)_2$	0.895	

Table 2

Parameters deduced from the fitted EXAFS spectra (N – coordination number, R – bond length, σ^2 – Debye-Waller factor, ΔE_0 – energy shift, R factor – goodness of fit).

Sample	$(Ni^{2+}–)X$	N	R (Å)	σ^2 (Å^2)	ΔE_0 (eV)	R factor
SG–His-OMe–Ni(II)	O/N	6	2.18	0.0153	3.40	0.0509
SG–Cys-OMe–Ni(II)	O/N	5	2.21	0.0112	0.40	0.0118
	S	1	2.64	0.0022		
SG–$(Cys\text{-}OMe)_2$–Ni(II)	O/N	6	2.19	0.0108	1.28	0.0139

Table 3

The SOD activities of the surface grafted complexes.

	IC_{50} (μM)
Cu,ZnSOD enzyme	0.4
SG–His-OMe–Mn(II)	31
SG–His-OMe–Mn(II)–H-His-OMe	26
SG–Cys-OMe–Mn(II)	39
SG–Cys-OMe–Mn(II)–H-Cys-OMe	30
SG–$(Cys\text{-}OMe)_2$–Mn(II)	32
SG–$(Cys\text{-}OMe)_2$–Mn(II)–$(H\text{-}Cys\text{-}OMe)_2$	29

Table 4 The conversion and selectivity results of the oxidation of cyclohexene (25 mg of catalyst, 5 mmol of cyclohexene + 1 mmol of peracetic acid dissolve in 10 cm^3 of acetone, 1 h reaction time at 298 K).

Catalyst	conversion (%)	cyclohexene oxide (%)	2-cyclohexen-1-ol (%)	2-cyclohexen-1-one (%)	cyclohexane-1,2-diol (%)
–	7	54	9	14	23
SG–His-OMe–Mn(II)	28	86	3	2	9
SG–His-OMe–Mn(II)–H-His-OMe	50	89	3	5	3
SG–Cys-OMe–Mn(II)	34	85	6	7	2
SG–Cys-OMe–Mn(II)–H-Cys-OMe	35	85	5	4	6
SG–$(Cys\text{-}OMe)_2$–Mn(II)	24	76	7	7	10
SG–$(Cys\text{-}OMe)_2$–Mn(II)–$(H\text{-}Cys\text{-}OMe)_2$	43	75	6	7	12

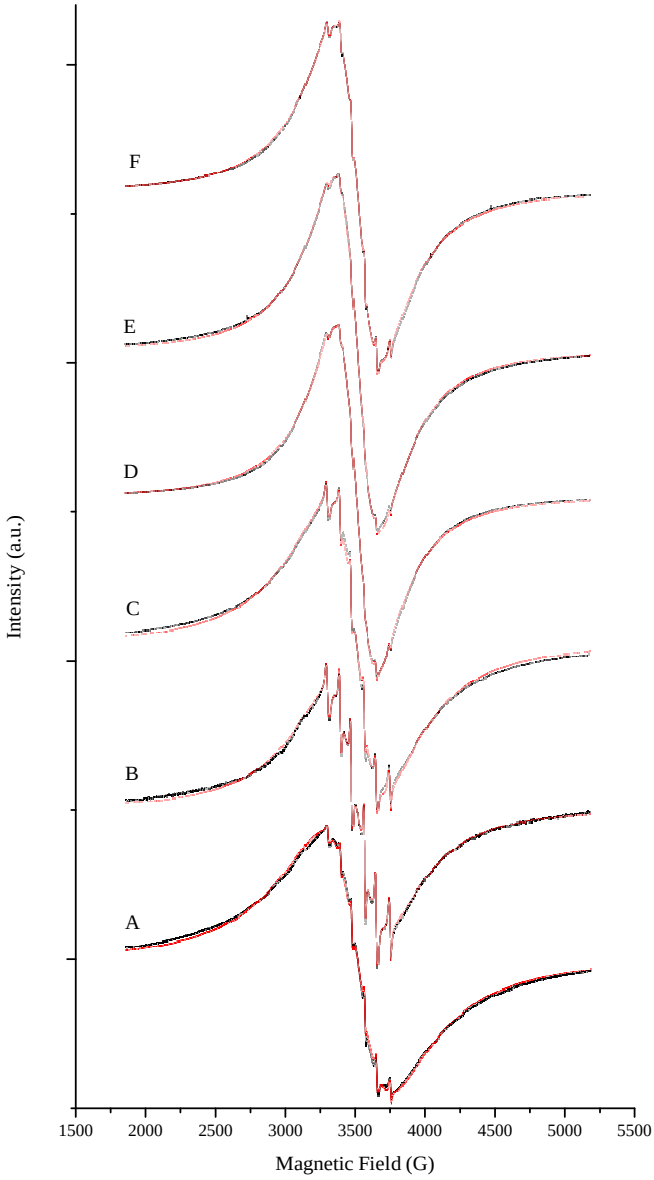
F
E
D
C
B
A
Intensity (a.u.)
1500
2000
2500
3000
3500
4000
4500
5000
5500
Magnetic Field (G)

Figure 1

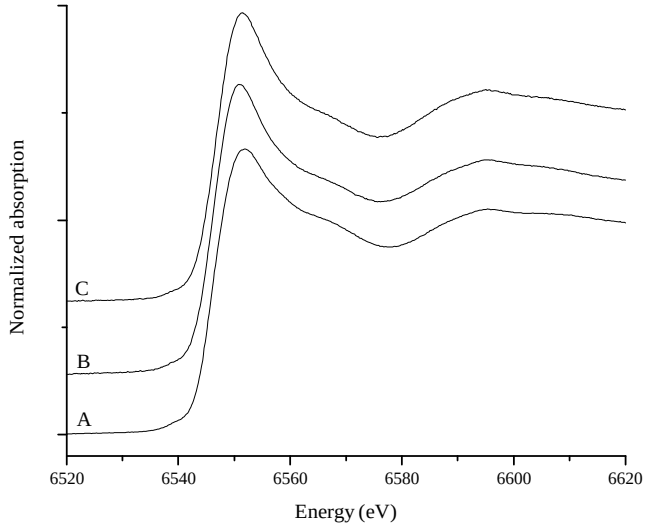
Normalized absorption
C
B
A
6520
6540
6560
6580
6600
6620
Energy (eV)

Figure 2

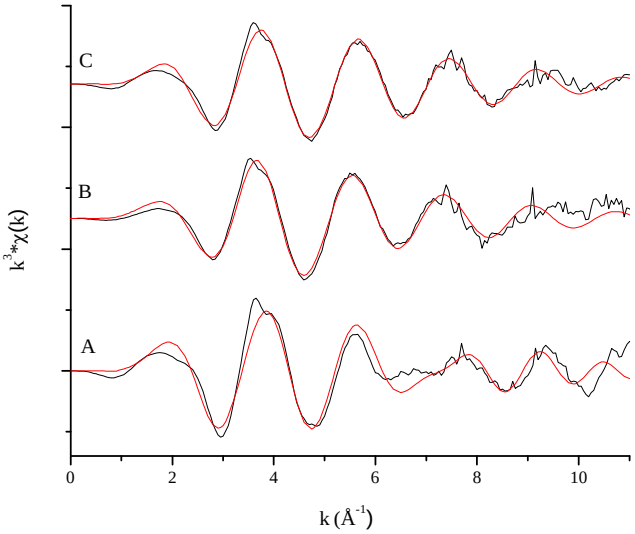

Figure 3

0 2 4 6 8 10

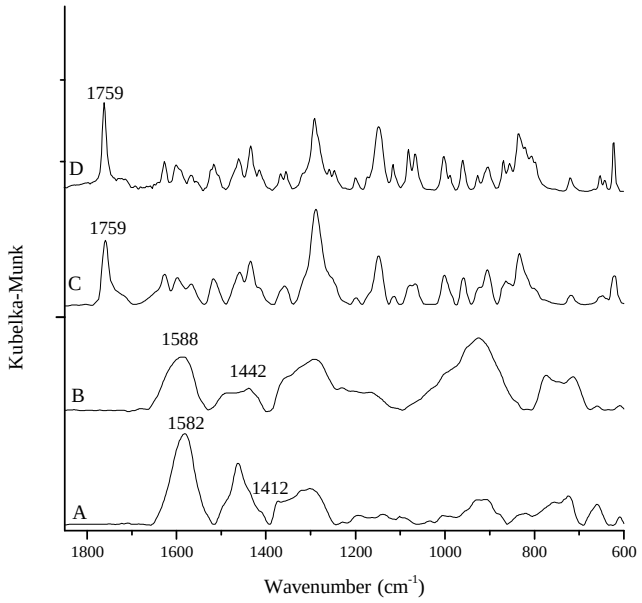
1759
D
1759
C
1588
1442
B
1582
1412
A
Kubelka-Munk
1800
1600
1400
1200
1000
800
600
Wavenumber (cm-1)

Figure 4

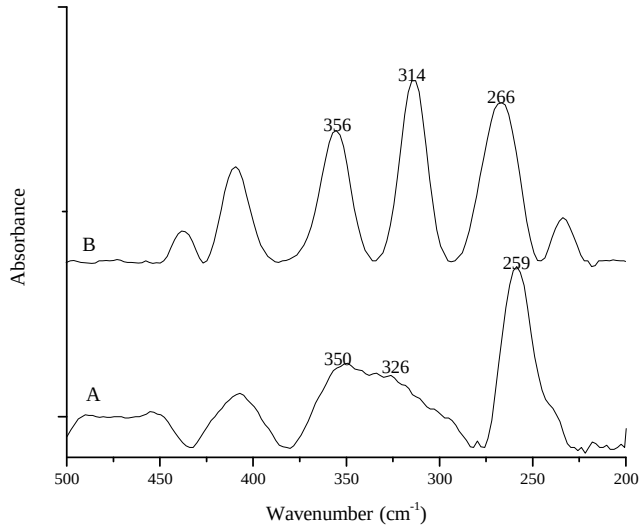
Absorbance
B
A
314
266
356
259
350
326
500
450
400
350
300
250
200
Wavenumber (cm-1)

Figure 5

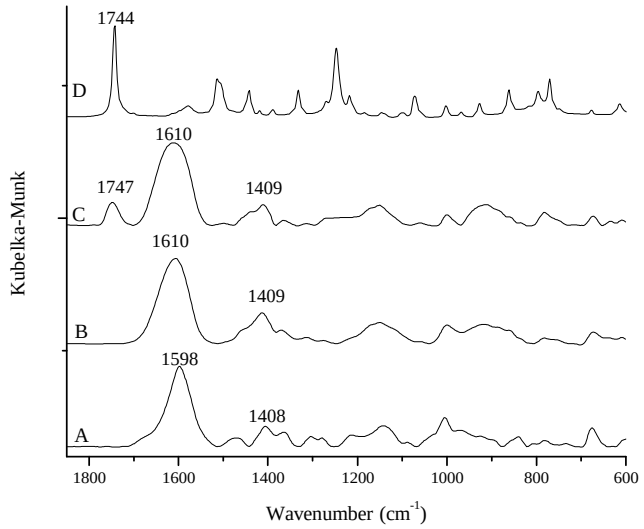
1744
D
1610
1747
1409
C
1610
1409
B
1598
1408
A
Kubelka-Munk
1800
1600
1400
1200
1000
800
600
Wavenumber (cm-1)

Figure 6

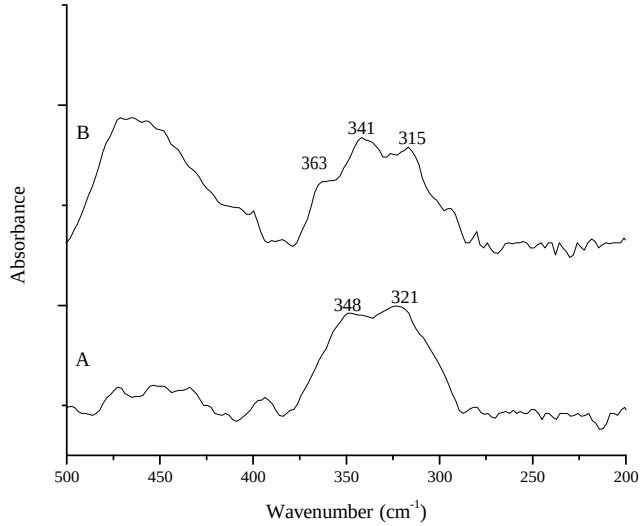
B
A
341
315
363
348
321
Absorbance
500
450
400
350
300
250
200
Wavenumber (cm-1)

Figure 7

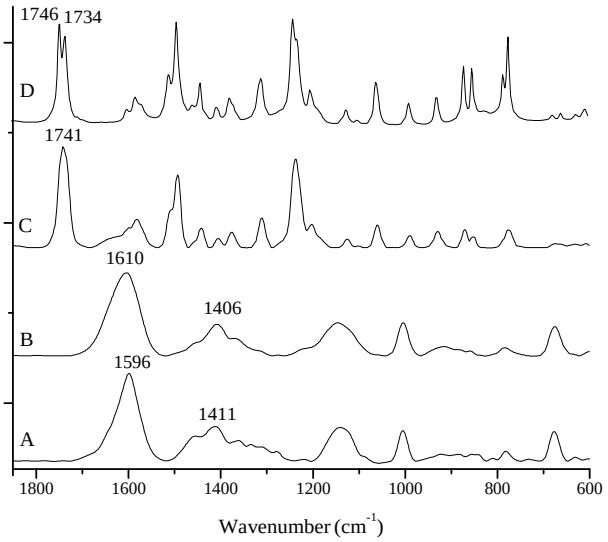
1746
1734
D
1741
C
1610
1406
B
1596
1411
A
1800
1600
1400
1200
1000
800
600
Wavenumber (cm-1)

Figure 8